

Synthetic areas spread in two-dimensional Superconducting Quantum Interference Arrays

R. D. Monaghan,¹ J. L. Marenkovic,¹ and G. C. Tettamanzi^{1,*}

¹*Quantum and Nano Technology Group (QuaNTeG),
School of Chemical Engineering, The University of Adelaide,
North Terrace Campus, Adelaide, 5005, South Australia, Australia*

(Dated: November 20, 2025)

Superconducting Quantum Interference Devices (SQUIDs), formed by incorporating Josephson junctions into loops of superconducting material, are the backbone of many modern quantum sensing systems. It has been demonstrated that, by combining multiple SQUID loops into a two-dimensional (2D) array, it is possible to fabricate ultra-high-performing Radio frequency sensors. However, to function as absolute magnetometers, current-in-use arrays require the area of each SQUID loop in the array to be incommensurate and, in turn, forbid the achievement of their full potential in terms of "quantum-limited" performances. This is because imposing incommensurability in the areas contrasts with optimised performance in each single SQUID loop. In this work, we report that by "selectively" inserting 'bare' sections of a superconducting circuit with no 'Josephson junctions', 2D SQUID arrays can operate as an absolute magnetometer even when no physical area spread is applied. Based on a generalisation of current available theories, a complete analytical formulation for the one-to-one correspondence between the distribution of these bare loops and what we call a "synthetic areas spread" is unveiled. This synthetic spread represents the equivalent physical spread of incommensurate SQUID loops that you will use to obtain the absolute Voltage-Magnetic Flux response if no bare loops were in use. Our work opens the way to a broader use of this technology for the fabrication of ultra-high-performance absolute quantum sensors. Our approach is also experimentally verified by fabricating several 2D SQUID arrays incorporating bare superconducting loops and by demonstrating that they behave in alignment with what is suggested by our theory.

Keywords: Josephson Effect, Quantum Sensing, Superconducting Quantum Interference Device (SQUID), Resistively-Shunted Junction (RSJ)

I. INTRODUCTION

The building block of superconducting based magnetometers is the superconducting quantum interference device (SQUID). In its most conventional implementation, i.e. the DC SQUID, this fundamental technology consists solely of a loop of superconducting material containing two Josephson junctions; a Josephson junction simply being a small barrier separating two superconducting regions¹. This technology has matured to several commercial applications such as the ones finalised to the operations of Magneto-Encephalography (MEG) machines². However, the Voltage-Magnetic Flux (VMF) response in conventional DC SQUIDs are highly noise sensitive and non-linear, making them impractical for some applications^{1,3–5}, especially when bandwidths in the Radio Frequencies (RF) ranges are needed. Because of this, as fabrication techniques improve, interest has turned to two-dimensional arrays of SQUID loops (i.e.; 2D SQUID arrays) that, by integrating a large number of SQUID cells in a serial and parallel electrical configuration, promise greater device sensitivity⁶, the ability to function as absolute magnetometers when appropriately designed and much more, while preserving all the other properties associated to superconductivity^{3–5}.

A problem with standard 2D SQUID arrays with identical loop areas is although they are sensitive to changes in the magnetic flux, they do not work as absolute magnetometers⁷. This renders this solution to the quantum

sensing problem more difficult to integrate in real systems. An improved solution to this problem exists and was put forward by Oppenländer *et al.* who found that, having the area of each SQUID loop (in the arrays) incommensurate to each other⁸, introduces interference between them^{3,9}. As a result, the oscillating voltages of each SQUID loop de-constructively interfere to produce an *anti-peak* response; a sharp dip in the voltage at zero-flux which allows the device to function as an absolute magnetometer. This can be easily understood as the incommensurate distribution of areas causing destructive interference effects for all non-zero flux values^{3,9–11}.

Indeed, the construction of 2D SQUID arrays with a spread in the distribution of area of the loops is certainly the cutting edge of the field⁵. However, an issue emerges which is that by varying the sizes of the loops – such as is done when spread in the areas is introduced – one also drastically changes the inductance L of each individual SQUID loop. The central parameter this modifies is known as β_L and is given by $\beta_L = LI_C/\Phi_0$, where I_C is the critical current of the component Josephson junctions, an Φ_0 is the quanta of magnetic flux². It has been determined experimentally that good control of β_L is critical to proper device performance¹². Although there have been proposals to mitigate this, it still posses a significant technological challenge for the fabrication of large 2D SQUID arrays with area spread.

In this paper we theoretically investigate (*and experimentally confirm*) a possible new solution to the prob-

lem; i.e.: the careful addition of ‘bare’ superconducting loops – loops of superconducting material containing **no** Josephson junctions – into the 2D SQUID array. We do so by first defining the mathematical framework required to study arrays of SQUIDs – namely, the RSJ equations. By replacing some of the SQUID loops with bare superconducting loops, we then study how the conventional RSJ equations of motion are modified. Finally, we present some experimental results for 2D SQUID arrays containing bare loops.

II. MODEL FOR SQUID ARRAYS

As shown in Fig. 1.a), our model explicitly consider a two-dimensional array of SQUIDs, with N horizontal loops, and M vertical loops; hence there $N \cdot M$ total SQUIDs within the array, and $M \cdot (N + 1)$ Josephson junctions. We assume the physical properties of each of these junctions, such as the resistance R and critical current I_C are constant across the array (and schematically included in the ‘x’ in Fig 1.a)). The overall dynamics of the array is determined^{2,3,13} by taking into account the phase difference across each Josephson junction of the array, φ . Correspondingly, for the i^{th} SQUID within the array the relevant parameters are the Josephson phase difference between the two Josephson junctions, $(D\varphi)_i$, and the physical area of each SQUID loop a_i .

To provide a mathematical model to study SQUID arrays, we make use of the RSJ equations¹. Although we leave further details to Appendix B and reference therein, the dynamics of the array can be summarised by solving^{2,3,13} the set of coupled equations as below;

$$\frac{d\varphi}{d\tau} = i^b - \sin \varphi + Q [D\varphi - a\Phi] , \quad (1)$$

where we have defined a unit-less time variable

$$\tau \equiv \frac{2\pi R I_C t}{\Phi_0} . \quad (2)$$

Each quantity in these equations 1 is defined in the Appendix B, however, each term can be ascribed to a physical origin^{2,3,13}: $\sin \varphi$ is the current term due to the first Josephson relation, the $\partial_\tau \varphi = \frac{d\varphi}{d\tau}$ is the derivative of the phase difference term due to the second Josephson relation, the i^b term is the current through each Josephson junction due to the bias current being applied, and $Q [D\varphi - a\Phi]$ is the (total) current due to inductive contributions. Concerning the dimensions, the vectors φ , and i^b contain $M \cdot (N + 1)$ elements as this is the total number of Josephson junctions, whilst $D\varphi$ and a contain $N \cdot M$ element as this is the total number of SQUIDs; Q , being a matrix, has a resulting dimension of $(M \cdot (N + 1)) \times (N \cdot M)$.

Given the physical parameters of each Josephson junction, Eq. 1 can be solved numerically to determine the

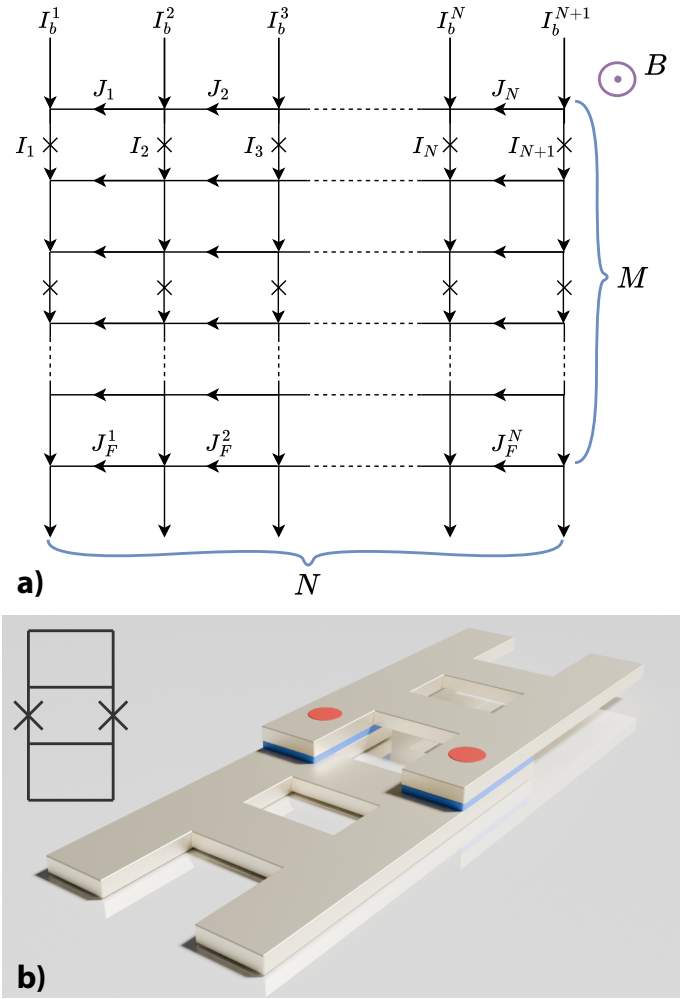


FIG. 1. a) Schematic of a prototypical 2D SQUID array containing both bare loops and SQUID loops. The numbering systems of the bias currents (I_b^i), the horizontal wires (J_i), the vertical wires (I_i), and the final row of horizontal wires (I_i^F) are labelled; the notation is identical to the circuit diagram of Ref.¹³ and is also described more in detail in the Appendix B. In this notation, two vertical wires $i-1$ and i with Josephson junctions will surround the generic i^{th} SQUID and the magnetic field \vec{B} is directed coming off the page. b) Illustration for a possible kind of unit-cell for the experimental array considered in this work. It consists of two bare loops surrounding a SQUID loop with the superconducting material shown in silver. Within the illustration, the red regions are vertical Josephson junctions, whilst the blue regions are made of insulating material. These junctions are normally shunted (not shown) in real circuits³⁻⁵. A circuit schematic for this cell is also in the top left side.

phase difference across each junction. We can then substitute this solution back into Eq. 1 to determine the voltage across each junction by the Josephson relation

$$V_i(\tau) = R I_C \frac{d\varphi_i}{d\tau} . \quad (3)$$

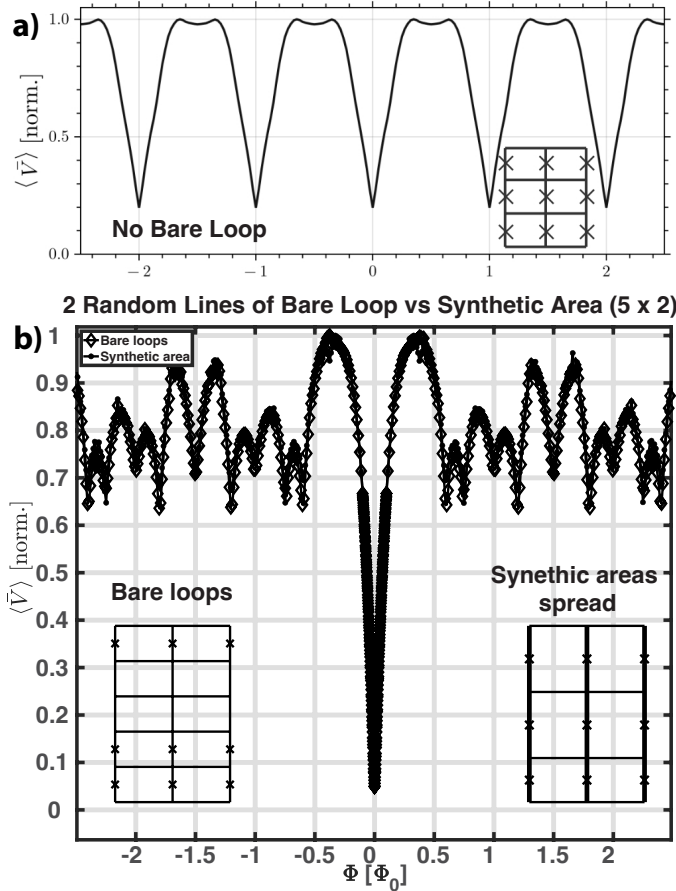


FIG. 2. (a) The Voltage-Magnetic Flux (VMF) response of a 3×2 array with equal loop areas is shown. (b) The VMF response of a 5×2 array containing two rows of solely bare loops is shown with black diamonds; each loop has an equal area as depicted in the circuit diagram. The VMF response of a 3×2 array where the loop area is given by the synthetic areas derived from the original circuit is overlaid; this was performed by solving Eq. 11. The schematics for these different situations are also shown in the figure.

Finally, by averaging the voltage over parallel junctions

$$\bar{V}(\tau) \equiv \frac{1}{N+1} \sum_i V_i(\tau), \quad (4)$$

we can compute the experimentally measurable time-averaged voltage by

$$\langle \bar{V} \rangle \equiv \lim_{T \rightarrow \infty} \frac{1}{T} \int_0^T \bar{V}(\tau) d\tau'. \quad (5)$$

III. SYNTHETIC AREA SPREAD

In this section we generalise model already present in the literature such as the ones recently published in ref.^{3,13}. Essentially, we will consider the dynamics of the

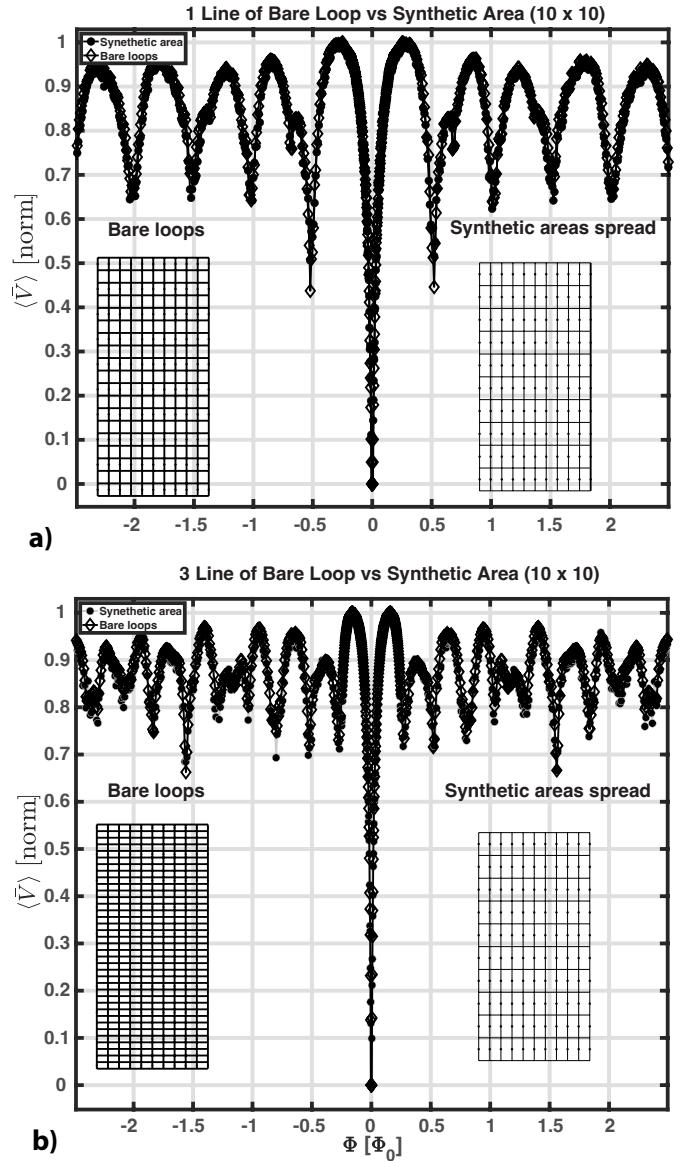


FIG. 3. Shown with the black empty diamonds is the Voltage-Magnetic Flux (VMF) response of a 10×10 array containing a) one or b) three rows of solely bare loops on each loop has an equal area as depicted in the left circuit diagram. Shown with the black full circles is the VMF response of arrays where the loop area is given by the synthetic areas derived from the two different configurations a) and b); this was performed by solving Eq. 11. For both these Figures, the differences between the bare loop and synthetic area approaches are minimal.

array outlined in Sec. II after removing Josephson junctions such that there exists loops within the array containing no Josephson junctions; we will call such loops 'bare' superconducting loops. We assume that of the previous $M \cdot (N+1)$ junctions, there are now N_{JJ} Josephson junctions remaining within the array. Similarly, we denote the number of remaining 'junction loops' – namely, loops containing at least a single Josephson junction – as N_{JL} , such that there are now the presence $N \cdot M - N_{JL}$

bare loops within the array.

We now differentiate whether a quantity corresponds to either a bare loop, or to a junction loop, by adding a subscript B , or J , respectively. For example, we let \underline{a}_J correspond to the vector containing the areas of all junction loops, whilst \underline{a}_B correspond to the area of all of the bare loops. The matrix Q is then partitioned into the form

$$Q = \begin{bmatrix} Q_{JJ} & Q_{JB} \\ Q_{BJ} & Q_{BB} \end{bmatrix}, \quad (6)$$

where the sub-matrix Q_{JJ} has dimension $(N_{JJ} \times N_{JJ})$ as it maps the flux through the junction loops into inductive current through the remaining Josephson junctions. We note that within this partition both $\underline{\varphi}_B = 0$ and $\underline{D\varphi}_B = 0$ by definition as there are no Josephson junctions to provide a phase difference. By partitioning each physical quantity in this manner, the equation of motion for the system is written as

$$\frac{d\underline{\varphi}_J}{d\tau} = \underline{i}_J^b - \sin \underline{\varphi}_J + Q_{JJ} \left[\underline{D\varphi}_J - \underline{a}_J \Phi \right] - Q_{JB} \underline{a}_B \Phi \quad (7)$$

Although this equation is similar to Eq. 1, the difference is the addition of the anomalous term $Q_{JB} \underline{a}_B \Phi$ which factors in the inductive current induced by the bare loops within the device.

We see from the structure of this equation that the matrix Q_{JJ} maps the magnetic flux through the N_{JJ} junction loops into the current across the N_{JJ} junctions; the precise nature of this mapping is constrained by Kirchhoff's law. However, as Kirchhoff's laws are overdetermined, then the rank of Q_{JJ} is equal to $\min(N_{JJ}, N_{JJ})$. For example, if there are two Josephson junctions shared between a single loop then by Kirchhoff's law the two currents are a function of the single flux value such that the rank of Q_{JJ} is identically one. Similarly, if there are instead two Josephson junctions shared between say three superconducting loops then by Kirchhoff's laws the current across the two junctions can be tuned independently by the extra flux value present such that $\text{rank}(Q_{JJ}) = 2$. The same logic applies to the total matrix $[Q_{JJ} \ Q_{JB}]$ such that

$$\text{rank}([Q_{JJ} \ Q_{JB}]) = \text{rank}(Q_{JJ}). \quad (8)$$

The purpose of illustrating this is because it implies that the columns of Q_{JB} must be a linear combination of the columns of Q_{JJ} , otherwise Eq. 8 would not be satisfied. Hence, we can introduce a coefficient matrix C such that

$$Q_{JB} = Q_{JJ}C. \quad (9)$$

The matrix of coefficients may not be unique in that the matrix problem defined by Eq. 9 may be underdetermined depending on the precise location of where the Josephson junctions have been removed. Regardless, we can substitute this into Eq. 7 to write the resulting equations of motion as

$$\frac{d\underline{\varphi}_J}{d\tau} = \underline{i}_J^b - \sin \underline{\varphi}_J + Q_{JJ} \left[\underline{D\varphi}_J - (\underline{a}_J + C\underline{a}_B) \Phi \right] \quad (10)$$

In Eq. 10 the area in the equations is no longer the physical area of each junction loop, given by \underline{a}_J , but instead a synthetic set of areas that has a synthetic spread of areas associated and as such containing a contribution from the bare loops areas \underline{a}_B . We denote this synthetic set of areas by \underline{a}'

$$\underline{a}' \equiv \underline{a}_J + C\underline{a}_B, \quad (11)$$

Eq. 10 is a fundamental result of this work as it demonstrates that the dynamics of array is determined by the synthetic set of areas, rather than the physical junction loop areas. An immediate consequence of this is that if all of the physical areas are identical, one would expect a periodic VMF response from the array⁹. However, by simply removing Josephson junctions from the array then the relevant parameter becomes the synthetic set of areas, which may also be engineered as incommensurate. Hence, the main result of this paper is the demonstrated ability to operate 2D arrays with the advantages of incommensurate spread of areas without varying the values of β_L (in fact β_L will be identical for every DC SQUID loop). As a result, we can obtain anti-peak responses without the need of physically modifying the areas or inductances of each individual SQUID loop and without risking the degrading of the performances of the 2D arrays when their size increase to large N and M as discussed in Ref.^{3,13}.

To explore this result we study different devices, **without losing any generality**, most of the results discussed in this works are for the case where only $I_{N/2+1}^b$ is $\neq 0$; also called central bias limit and without any forms of noise included into the model. Initially, a small device consisting of six SQUID loops and containing two columns and three rows is numerically considered. In Fig. 2.a), we plot the time-averaged voltage for this array when every loop area is the same size. This is a well-known results; the response is characteristically periodic as there is no interference induced by the different SQUID loops³.

In Fig. 2.b) we plot the response of two different devices: one, plotted with black diamonds, containing two rows of bare loops and all the loops having the same sizes, whilst the data plotted with black full circles are for the equivalent circuit with the synthetically defined spread of the area loops. For this example, the areas of the bare device are identical, however, by solving Eq. 11 we find that the areas of the equivalent device are given by the following sequence; $\underline{a}' = [\frac{3}{2} \ \frac{3}{2} \ \frac{3}{2} \ \frac{3}{2} \ 1 \ 1]$ in units of the area used for the bare loops original structure. We observe a very slight discrepancy between the two as the inductances of the two devices may differ slightly and also because we make no effort in optimising the bias current for the plot, however, visually the interference produced is almost identical. As also seen in the Fig. 2.b), due to the presence in the circuit of the two lines of bare loops, both have a periodicity around $0.5 \Phi_0$ which is half of the periodicity for the case without bare loop. This is essentially a manifestation of the fact that, in our plots, we

are using the magnetic flux that goes in each DC SQUID loop as a references for the x-axis, even when extra bare loops are introduced into the circuit. This in turn means that DC SQUID are synthetically varied by the presence of the bare loops. Hence, this section confirms that by using the local careful positioning of bare loops an centrally peaked VFM response can be obtained even without the need of imposing a physical spread in the areas.

In Fig. 3 another pair of devices where we take devices with a 10×10 array and incorporating a) one or b) three rows of solely equal area bare loops are theoretically investigated. Again solving Eq. 11, we can find the sequence for the synthetic areas of the equivalent devices, these are shown in Appendix A. Most important the ones in Figure 3 are just two others of the many possible examples that can be used to demonstrate the very powerful concepts of synthetic area spread which is introduced in this paper. The same identical curves as in Figure 3 a) and 3b) are shown with a much broader Magnetic Flux range in Fig. 3 of Appendix E. These extra data demonstrates that it is fairly easy to define a bare loop configuration, with no physical spread, but for which the equivalent synthetic spread results in a singular global minimum at zero flux. Hence, it is always possible to define devices that manifests an absolute zero, as opposed to that of a conventional DC SQUID response³⁻⁵, without the need of using performance degrading techniques. Lastly, the robustness vs scaling with number of loops is also investigated in Fig. 4 of the Appendix E by showing that even for a SQUID array containing 64×64 DC SQUID loops and one, two or three lines of bare loop incorporated between each line of DC SQUIDs, the average Voltage Difference between the array with bare loop and the correspondent synthetic area arrays, calculated without any optimisation in the bias currents, is always maintained to a minimal value.

IV. EXPERIMENTAL RESULTS

As demonstrated in Fig. 4 and Fig. 5 (and Fig. 1 and Fig. 2 in Appendix E), arrays without physical spread in the distribution of the area have been fabricated to test our theoretical assumptions; some containing bare loops and some with no-bare loops. While the details of the fabrication methods for these devices are described in the Appendix D, it is important to remind here that each fabricated device consist of array formed by the unit-cell depicted in Fig. 1; consisting of a number $N \times N$ single SQUID loops. For some devices, as in Fig. 4 (and Fig. 1a in Appendix E) each horizontal line of SQUID loops (i.e.; 1 to N in Fig. 1) is sandwiched between two lines of bare superconducting loops. In the case of the ones with bare loop, the area of the SQUID loop was twice that of the bare superconducting loop. This unit-cell was then repeated within a 16×16 array to produce a 2D SQUID array containing also rows of bare loops. As a result, the total device consisted of sixteen hori-

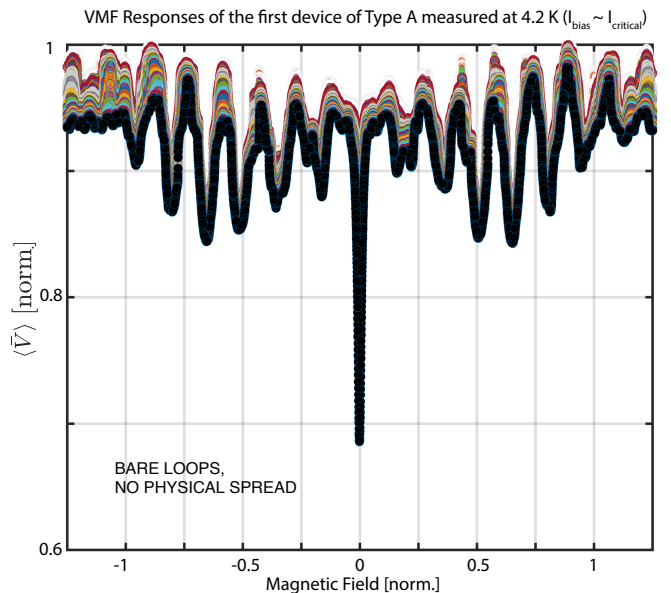


FIG. 4. Experimental VMF curves, for different biases close to the critical one, for the type A 16×16 device consisting of the unit-cell depicted in Fig. 1 and with two lines of bare loops between each line of SQUIDs. Although all the SQUID loops and all the bare loops in this structure have identical areas, a strong anti-peak response visible indicates the appearance of synthetic loop areas induced by the bare loops present in the circuit. The data for a device with an identical design and a demonstrated identical low temperature response are shown in Fig. 2 of Appendix E.

zontal loops and forty-eight vertical loops. Opposite to this, devices as in Fig. 5 (and Fig. 1b in Appendix E) are made of horizontal lines of SQUID loop vertically connected **without any lines of bare loops in between**. Indeed, to probe the voltage response of these devices, an external superconducting coil was used to apply a homogenous magnetic field through each of the arrays. A pair of leads allows one to apply a bias current in order to bring the device towards the correct resistive mode for device operation, but also allows the voltage drop across the array to be measured. It is worth noting that the magnetic field range of x-axis for every experimental plot is limited by the maximum amount of current that can be sustained by the coils used to generate the applied magnetic fields. It is also important to outline here that the experimental setup is similar to the theoretical situation of central bias limit discussed in Fig. 2 and Fig. 3. By sweeping the external current through the coil, the characteristic Voltage-Magnetic Flux (VMF) curve for each device can be measured. The typical experimental VMF response for our devices is plotted in Fig. 4. We note that (as also shown in the Appendix E) this curve was highly reproducible with multiple devices with identical design chosen at random across the wafer. For the curves shown, the bias current was tuned such that the best anti-peak response was observed. It is also important

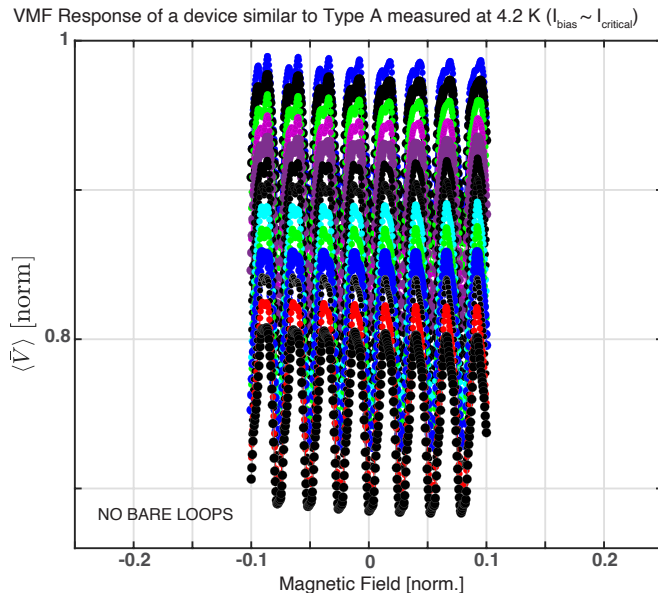


FIG. 5. Experimental VMF curves for different biases close to the critical one and for a device that has a similar design (but not identical) as the one in Figure 4, but **no bare loops**. As expected, the VMF curves of the device are not anti-peaked.

to note that the x- and y-axes of all the experimental data have been normalised identically, as, in this work, we are uniquely interested in the general manifestation of the effect we are discussing. The striking behaviour of this measurement is the appearance of a significant anti-peak – the drop in the measured voltage around zero flux. Indeed there are no additional significant minima as the strength of the external magnetic field is increased. Concerning the discussion in Sec. III, in Fig. 5 (and identically in Fig. 1b of Appendix E), we consider a separate 2D SQUID array which contains no bare loops and observe that no central anti-peak is observed in this case. Hence, we have illustrated theoretically and experimentally that the careful addition of bare loops can be used to dramatically modify the VMF response in our 2D SQUID arrays. In this section, the experimental data represent a qualitative realisation of the effect, as we don't exclude that other effects (e.g. device imperfections) may have played a (minor) role in the way experimental results have manifested; **however, they are confirming that the physics that dominates the response is linked to the core results of this work; bare loops and the corresponding synthetic areas generated by these will define the absolute response of our devices.**

V. SUMMARY AND OUTLOOK

This work demonstrates a novel method that can be used to modify the response of 2D SQUID arrays towards

an ideal one, without degrading their performances. It not only has the merit to broaden the state-of-the-art theoretical results, **but, most importantly, provides a clear analytical and numerical explanation on how to reproduce this absolutely central effect**, opening the way to its routine use. The central message of this work is that it provides a fully analytical, numerical and experimental demonstration of the new concept of synthetic area spread, which, by locally placing bare loops of superconducting materials and incorporating them ad hoc in the superconducting arrays of DC SQUIDs can operate these systems as absolute magnetometers without degrading their performances; hence, this may finally open the way to ultra-performant integrated sensors for electromagnetic signals. In conclusion, the importance of this work is that it has the potential to finally unlock the ability of the SQUID arrays technology towards the quantum limit of detection of electromagnetic signals.

VI. DATA AVAILABILITY

All relevant data presented in the paper are available upon reasonable request.

VII. CODE AVAILABILITY

All computer code used in the paper is available upon reasonable request.

ACKNOWLEDGMENTS

The research was partially supported by the University of Adelaide via the CAS funding scheme. R. D.M., J. L. M. and G. C. T are supported by the Australian Commonwealth Government through Research Training Program Scholarships. J. L. M. is also funded via the Ian Croser Research Scholarship in Engineering at the University of Adelaide. G.C.T. conceived the project. R. D.M. performed the analytical and numerical calculations with input from all authors. The concept of Synthetic Spread of the Areas and the subsequent idea of Mixed SQUID arrays are the subject of an international patent application no. PCT/AU2025/050991. We acknowledge discussion with T. Whittaker concerning the nature of the bare loops & the interpretation of the exp. data and A. Gardin for the production of Fig. 1b).

* giuseppe.tettamanzi@adelaide.edu.au

- ¹ M. Tinkham, *Introduction to Superconductivity*, International Series in Pure and Applied Physics (McGraw-Hill, New York, 1975).
- ² H. Weinstock, ed., *SQUID Sensors: Fundamentals, Fabrication and Applications* (Springer Netherlands, Dordrecht, 1996).
- ³ J. Oppenlander, C. Haussler, T. Trauble, P. Caputo, J. Tomes, A. Friesch, and N. Schopohl, IEEE Transactions on Applied Superconductivity **13**, 771 (2003).
- ⁴ E. E. Mitchell, K. E. Hannam, J. Lazar, K. E. Leslie, C. J. Lewis, A. Grancea, S. T. Keenan, S. K. H. Lam, and C. P. Foley, Superconductor Science and Technology **29**, 06LT01 (2016).
- ⁵ V. K. Kornev, I. I. Soloviev, N. V. Klenov, and O. A. Mukhanov, "High linearity superconducting radio frequency magnetic field detector," (2015), <https://patents.google.com/patent/US9588191B1/en>.
- ⁶ Sensitivity in a SQUID array is sometime more specifically associated in the literature to the concept of transfer function $\frac{dV}{dB_{Ext}}$ or to the one of Noise Sensitivity sometimes expressed in $\frac{PT}{\sqrt{Hz}}$, we are here just mentioning sensitivity in its broader sense which may include both these concepts.
- ⁷ C. Häussler, J. Oppenländer, and N. Schopohl, Journal of Applied Physics **89**, 1875 (2001), https://pubs.aip.org/aip/jap/article-pdf/89/3/1875/19218121/1875_1_online.pdf.
- ⁸ No lowest common divisor exists.
- ⁹ J. Oppenländer, Ch. Häussler, and N. Schopohl, Physical Review B **63**, 024511 (2000).
- ¹⁰ S. A. Cybart, T. N. Dalichaouch, S. M. Wu, S. M. Anton, J. A. Drisko, J. M. Parker, B. D. Harteneck, and R. C. Dynes, Journal of Applied Physics **112**, 063911 (2012).
- ¹¹ F. Couëdo, E. Recoba Pawłowski, J. Kermorvant, J. Trastoy, D. Crété, Y. Lemaître, B. Marcilhac, C. Ulysse, C. Feuillet-Palma, N. Bergeal, and J. Lesueur, Applied Physics Letters **114**, 192602 (2019).
- ¹² B. Chesca, R. Kleiner, and D. Koelle, "Squid theory," in *The SQUID Handbook* (John Wiley and Sons, Ltd, 2004) Chap. 2, pp. 29–92, <https://doi.org/10.1002/3527603646.ch2>.
- ¹³ M. Galí Labarias, K.-H. Müller, and E. Mitchell, Physical Review Applied **17**, 064009 (2022).
- ¹⁴ SEEQC, *2024 Conservative Design Rules*, Tech. Rep. (2024).

Appendix A: Synthetic areas

The sequences for the synthetic area spreads for Fig. 3 are listed below. For the device with 1 line of bare loops pictured in Fig. 3 a) the sequence of synthetic areas is

given by

1.36	1.46	1.49	1.49	1.49	1.49	1.49	1.49	1.46	1.36
1.73	1.92	1.98	1.99	1.99	1.99	1.99	1.98	1.92	1.73
1.73	1.92	1.98	1.99	1.99	1.99	1.99	1.98	1.92	1.73
1.73	1.92	1.98	1.99	1.99	1.99	1.99	1.98	1.92	1.73
1.73	1.92	1.98	1.99	1.99	1.99	1.99	1.98	1.92	1.73
1.73	1.92	1.98	1.99	1.99	1.99	1.99	1.98	1.92	1.73
1.73	1.92	1.98	1.99	1.99	1.99	1.99	1.98	1.92	1.73
1.73	1.92	1.98	1.99	1.99	1.99	1.99	1.98	1.92	1.73
1.73	1.92	1.98	1.99	1.99	1.99	1.99	1.98	1.92	1.73
1.36	1.46	1.49	1.49	1.49	1.49	1.49	1.49	1.46	1.36

Similarly for the device with 3 lines of bare loops pictured in Fig. 3 b), the sequence of synthetic areas is given by

1.80	2.17	2.34	2.41	2.44	2.44	2.41	2.34	2.17	1.80
2.60	3.34	3.68	3.83	3.89	3.89	3.83	3.68	3.34	2.60
2.60	3.34	3.68	3.83	3.89	3.89	3.83	3.68	3.34	2.60
2.60	3.34	3.68	3.83	3.89	3.89	3.83	3.68	3.34	2.60
2.60	3.34	3.68	3.83	3.89	3.89	3.83	3.68	3.34	2.60
2.60	3.34	3.68	3.83	3.89	3.89	3.83	3.68	3.34	2.60
2.60	3.34	3.68	3.83	3.89	3.89	3.83	3.68	3.34	2.60
2.60	3.34	3.68	3.83	3.89	3.89	3.83	3.68	3.34	2.60
2.60	3.34	3.68	3.83	3.89	3.89	3.83	3.68	3.34	2.60
2.60	3.34	3.68	3.83	3.89	3.89	3.83	3.68	3.34	2.60
1.80	2.17	2.34	2.41	2.44	2.44	2.41	2.34	2.17	1.80

Appendix B: Mathematical model of 2D SQUID arrays

To determine the equivalence between 2D SQUID arrays containing bare loops with no area spread, and those with area spread and no bare loops, we must first choose a formalism to work with. To this end we will make use of a circuit theory approach utilising the RSJ equations¹. We will adopt the matrix formalism introduced in Ref.¹³, however, we will extend their results to factor in the introduction of bare superconducting loops.

In Fig. 1a) we depict a schematic of the prototypical 2D SQUID array studied within this work. It consists of M superconducting loops in the vertical axis, and N loops in the horizontal axis. Some of these loops of superconducting wire have two Josephson junctions along their vertical sides, hence forming SQUID loops; the remaining loops which do not contain Josephson junctions we denote as 'bare' superconducting loops. Indeed this generalised 2D SQUID array can be considered as a standard SQUID array where interspersed with bare superconducting loops. In the specific example shown in Fig 1a), we see that the first, third, and final rows consist of SQUID loops, whilst the second and penultimate rows contain solely bare loops. This configuration in Fig. 1a) is one example and other more specific cases described in this papers. It indeed important to outline here that our modelling approach is quite general and that the examples discussed

in this work will represent only a sub-set of what is possible to model with it.

We denote the current through the k^{th} vertical wire segments as I_k , where, reading from left to right and top to bottom, we number each wire sequentially; only the first $N + 1$ vertical wire segments are labelled in the figure. For the horizontal wire segments we denote them by J_k and also label them sequentially, however, we distinguish the final row of horizontal currents by labelling them as J^F_k . We will denote the vectors containing each of these elements by the underlined quantities \underline{I} , \underline{J} , \underline{I}^b , \underline{J}^F . Concerning dimensions: \underline{I} contains $M \cdot (N + 1)$ elements, \underline{J} contains $N \cdot (M - 1)$ elements, \underline{J}^F contains N elements, and we pad \underline{I}^b with $(N + 1) \cdot (M - 1)$ zeros ($\underline{I}^b \equiv [I^b_1, \dots, I^b_{N+1}, 0, \dots, 0]^t$) such that the resulting vector has the same length as \underline{I} .

Within a circuit theory, one can construct Kirchhoff's current conservation laws at each vertex of the circuit. For example, the conservation condition for the vertex located at the intersection between the i^{th} column and the j^{th} row, assuming it is not lying on the edge of the graph, is given by

$$I_{i+(j-1)(N+1)} = J_{i+(j-1)N} + I_{i+(j-2)(N+1)} - J_{i-1+(j-1)N}. \quad (\text{B1})$$

Following the work of Ref.¹³, we introduce coefficient matrices K^I and K^J consisting entirely of -1 , 0 , and 1 such that the Kirchhoff conservation condition for every node can be represented as the matrix equation

$$K^I \underline{I} = K^J \underline{J} + \underline{I}^b. \quad (\text{B2})$$

where K^I has dimensions $[M \cdot (N + 1) \times M \cdot (N + 1)]$ and K^J has dimensions $[M \cdot (N + 1) \times N \cdot (M - 1)]$.

As we distinguished the final row of horizontal currents, we must also introduce further Kirchhoff matrices N_I , with dimension $[N \times M \cdot (N + 1)]$, and N^F , with dimension $[N \times N]$, defined such that the current conservation laws for the final row of vertices are contained within the system of equations

$$\underline{J}^F = N^I \underline{I} + N^F \underline{I}^F. \quad (\text{B3})$$

where $\underline{I}^F \equiv [I^b_1, \dots, I^b_N]^t$ bundles the currents leaving the device into a vector.

The current through each wire segment will in-turn produce an inductive flux contribution through each superconducting loop, which we denote by the vector $\underline{\Phi}^L$ containing $N \cdot M$ elements. To determine the flux contributions resulting from these vertical (\underline{I}), horizontal (\underline{J}), and final row (\underline{J}^F) we must introduce inductance matrices L^I , L^J , L^F respectively. Although the precise form of these matrices will be determined by the physical model for the inductances considered i.e. kinetic inductances, geometric inductances, they give the resulting inductive contribution to the flux through each loop by

$$\underline{\Phi}^L = L^I \underline{I} + L^J \underline{J} + L^F \underline{J}^F. \quad (\text{B4})$$

Due to the phase quantisation condition for each superconducting loop, this inductive contribution to the flux

is balanced by both the external flux through that loop, Φ^{ext} , and any Josephson junction phase differences φ present within that loop. However, in a bare superconducting loop there are no Josephson junction phases to balance the external flux; this is the critical distinction between a bare loop and a SQUID loop. Without the loss of generality, for the i^{th} loop in the array surrounded generically by the $k - 1$ and k vertical wire segments, the corresponding phase quantisation conditions through the SQUID loop and the bare loops are given by

$$\begin{aligned} \text{SQUID : } \Phi^{\text{ext}} + \Phi_i^L &= \varphi_k - \varphi_{k-1} \equiv (D\varphi)_i, \\ \text{bare : } \Phi^{\text{ext}} + \Phi_i^L &= 0. \end{aligned} \quad (\text{B5})$$

At the expense of introducing more notation, it is useful to introduce sets \mathcal{S} and \mathcal{J} defined as

$$\begin{aligned} \mathcal{S} &\equiv \{i \mid \text{the } i^{\text{th}} \text{ loop is a SQUID}\}, \\ \mathcal{J} &\equiv \{k \mid \text{the } k^{\text{th}} \text{ vertical wire forms part of a SQUID}\}, \end{aligned} \quad (\text{B6})$$

to allow us to distinguish notationally between wires and loops forming SQUID loops. The number of elements of these sets are precisely the number of SQUID loops, and the number of Josephson junctions, which we label as N_{SQUID} and N_{JJ} respectively. We can now compactly write the phase quantisation conditions for SQUIDS and bare loops defined by Eq. B5 in vector form as

$$\underline{\Phi}^{\text{ext}} + \underline{\Phi}^L = \underline{\theta}, \quad (\text{B7})$$

where we have introduced a generalised difference vector $\underline{\theta}$ whose elements are defined by

$$\theta_i = \begin{cases} (D\varphi)_i & i \in \mathcal{S}, \\ 0 & i \notin \mathcal{S}. \end{cases} \quad (\text{B8})$$

With the aim of rewriting the inductive contribution within Eq. B7 as a function of the currents through the device, we combine the Kirchhoff matrices defined previously with the inductive flux contribution defined in Eq. B4 to express the phase quantisation condition as a function of solely the horizontal currents \underline{J}

$$\underline{\Phi} + L \underline{J} = \underline{\theta}, \quad (\text{B9})$$

where

$$\begin{aligned} L &\equiv L^J + (L^I + L^F N^I) K^{I-1} K^J, \\ \underline{\Phi} &\equiv \Phi^{\text{ext}} + (L^I + L^F N^I) K^{I-1} \underline{I}^b + L^F N^F \underline{I}^F. \end{aligned} \quad (\text{B10})$$

The dynamics of each Josephson junction is a function of not only both the phase difference across that junction, φ_k , and the current I_k , but also the physical parameters such as the resistance R , and the critical current I_C of each junction. Assuming identical over-damped Josephson junctions, the relationship between the current through each junction and the phase difference φ is given by the RSJ model¹

$$\frac{I_k(t)}{I_C} = \sin \varphi_k(t) + \frac{\Phi_0}{2\pi R I_C} \frac{d\varphi_k}{dt}, \quad k \in \mathcal{J}. \quad (\text{B11})$$

Note that we have omitted a noise and further capacitive term, which, although are standard terms to include for the purposes of modelling, are irrelevant in proving the equivalence between arrays containing bare loops and no spread, and arrays containing area spread but no bare loops.

As the RSJ equations require only the currents through the Josephson junctions, rather than through every wire segment, we introduce a mask matrix M with dimensions $[N_{JJ} \times M \cdot (N+1)]$ which can project vectors defined over every wire segment onto vectors defined only over wire segments containing a Josephson junction. The elements of this projection matrix are defined as

$$M_{ij} = \delta_{j, \mathcal{J}_i}, \quad (B12)$$

such that the vector of currents through each Josephson junction is given by $M\underline{I}$. Substituting in Eq. B9 and the Kirchhoff matrices, taking account of the presence of the bias currents \underline{I}^b , and through the use of the projection matrix M , we can now express the RSJ equations defined in Eq. B11 as

$$\frac{d\varphi}{d\tau} = \underline{C} + KL^{-1} [\theta - \underline{\Phi}] - \sin \varphi, \quad (B13)$$

where we have defined

$$\begin{aligned} \tau &\equiv \frac{2\pi RI_C t}{\Phi_0}, \\ \underline{C} &\equiv (MK^{I^{-1}}\underline{I}^b)/I_C, \\ K &\equiv (MK^{I^{-1}}K^J)/I_C. \end{aligned} \quad (B14)$$

to simplify the resulting equation. Eq. B13 is the equation of motion for a 2D array containing bare loops, whereupon all dynamics can be evaluated by solving this equation.

Appendix C: Rank of sub-matrices

In this section we consider the rank of the sub-matrices of Q defined by

$$Q \equiv K^{I^{-1}}K^J L^{-1}, \quad (C1)$$

Importantly, K_I and L are invertible and hence full rank. As a result the rank of Q is simply given by the rank of K_J

$$\text{rank}(Q) = \text{rank}(K_J), \quad (C2)$$

Appendix D: Fabrication Methods

The experimental data of several device fabricated by SEEQC Ref.¹⁴ using a typical fabrication process

for niobium-based superconducting integrated circuits. This uses only refractory materials, with the exception for a Pd/Au metallisation layer used for contact pads. Niobium is used as the superconducting material due to its comparably high critical temperature, electrical and thermal stability, and ability to be thermally cycled many times without degradation. Niobium/Aluminum-Oxide/Niobium Josephson tunnel junctions are made by depositing an in-situ trilayer across the entire wafer and subsequently defining junction areas by deep-UV photolithography and etching. This method yields good uniformity and reproducibility of junction parameters. The critical current density of Nb/AlOx/Nb tri-layer associated with these devices is 4.5 kA/cm². The Josephson junctions are interconnected into circuit configurations using four superconducting layers: junction base electrode (layer M1), two Nb wiring layers (layers M2 and M3), superconducting Nb ground plane (layer M0) and a NbNx high-kinetic-inductance layer below the ground plane (MN1). The sheet resistance of the resistive layer (R2) is a Ti/PdAu/Ti resistive material with sheet resistance of 4.0 ohms/sq. Low loss SiNx is used is deposited to provide insulation between the conducting layers. Anodisation of the base electrode of tri-layer provides additional insulation to Josephson junctions. The wafer used for the devices is fabricated on a 150-mm diameter (6-inch) high resistivity Si wafers.

Many different devices, starting from single Josephson Junction to DC SQUIDs and more complicated Nb devices have been fabricated and measured and have demonstrated very high reproducibility as expected for this technology¹⁴. A total of around ten devices with no spread have been measured at temperatures between 4.2 K to 8 K; two of them seem to be not responding to both Voltage Current and Voltage Flux measurement when studied. The data of most all the others devices demonstrates high reproducibility and are discussed either in the main document or in these Appendices. Hence, approximatively 80 % of the devices used for this study are operating correctly (while the others are simply not operating at all). Conventional ultra-low noise setup is used to measure Voltage-Current and Voltage-Magnetic Flux curves. Many devices of different geometries have been successfully measured, in this work we are focusing on the ones that have used the bare loop configuration.

Appendix E: More Results

More theoretical and experimental results linked to the discussion in the main section of the paper are listed below.

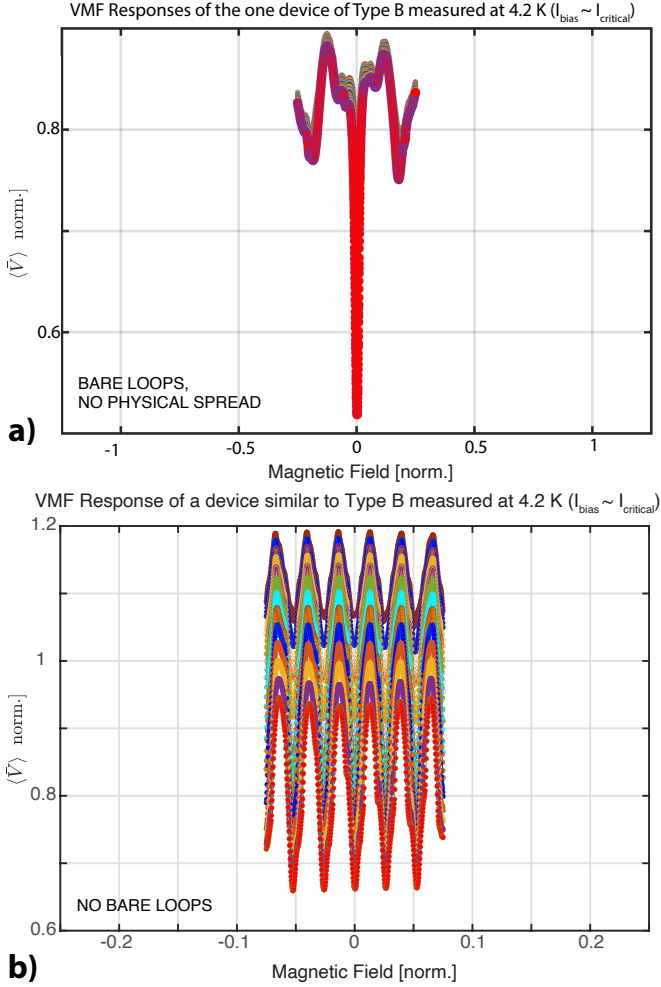


FIG. 6. Experimental VMF curves (for different biases close to the critical one) for the type B 16×16 of a different device (i.e.; shunting resistance in each junction is 9.6 Ohm as opposed to 7.2 Ohm in the device of Fig. 4 in the main section of the paper), if compared to the one in Fig. 4 of the paper and consisting of the unit-cell depicted in Fig. 1 of the paper and with only two lines of bare loops. Same as before, a strong anti-peak response visible indicates the appearance of the synthetic loop areas induced by the bare loops present in the circuit. The device, as in b), has a very similar design (although not identical) to the first but no bare loops. As expected, the VMF of the second device is not anti-peaked.

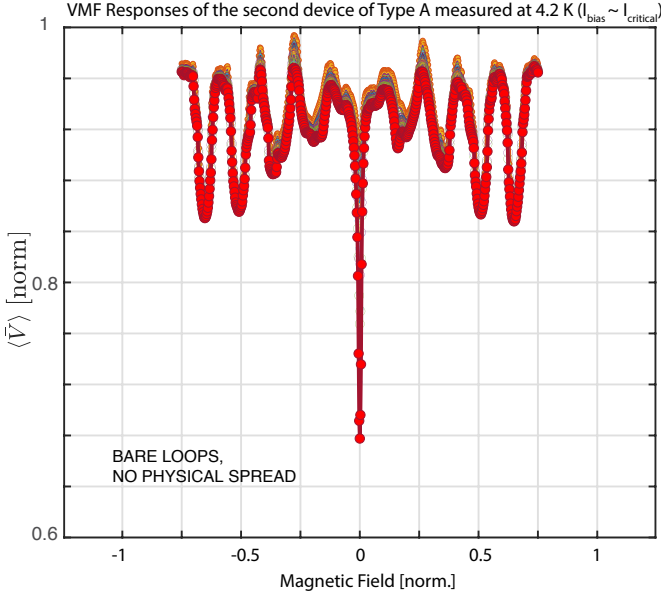


FIG. 7. Experimental VMF curves (for different biases close to the critical one) for the type A 16×16 of a different device of Type A identical to the one discussed in Fig. 4 in the main section of the paper.

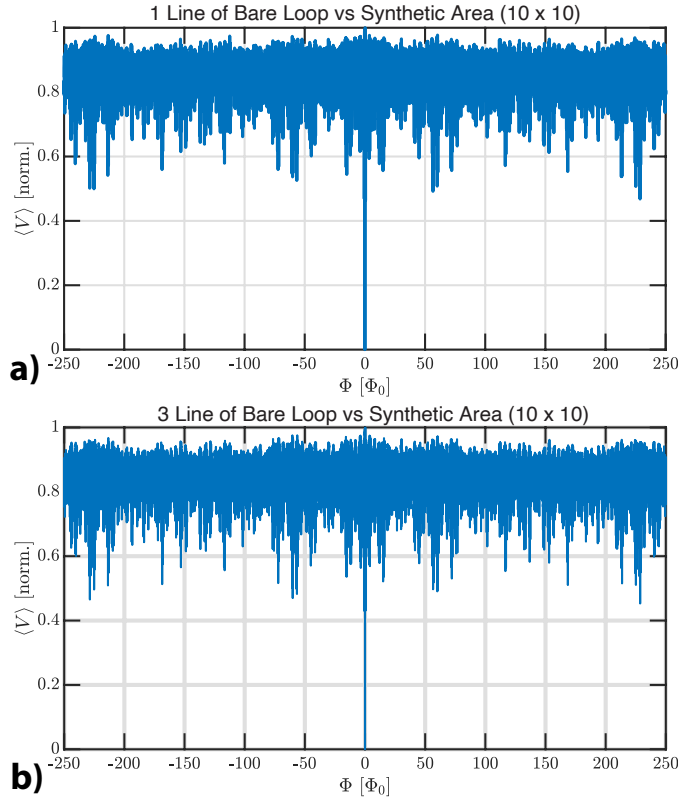


FIG. 8. Shown with the blue lines are the Voltage-Magnetic Flux (VMF) response with a wide range of magnetic quantum fluxes (± 250) of a) the same devices as in Fig. 3a) of the in the main section of the paper or b) the same devices as in Fig. 3b) in the main section of the paper.

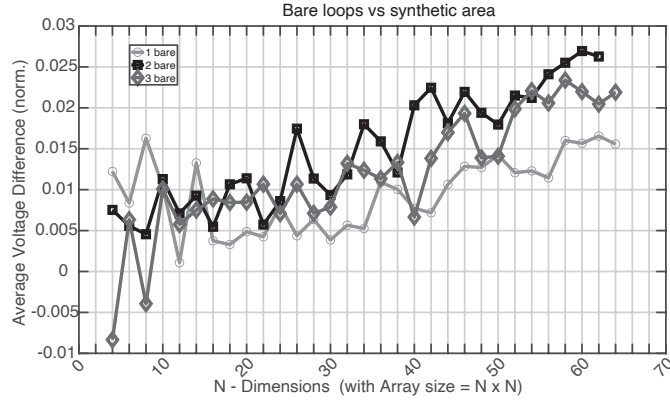


FIG. 9. By showing the difference in the theoretical Voltage Response, this figure illustrates the robustness in accuracy of the VMF response for devices with bare loops vs synthetic area, even for $N \times N$ close to 64×64 and one, two or three lines of bare loops incorporated between lines of DC SQUIDs. These results expand the one of Fig. 3 in the main section of the paper.